AIP | Applied Physics Letters

Can p-channel tunnel field-effect transistors perform as good as n-channel?

A. S. Verhulst, D. Verreck, M. A. Pourghaderi, M. Van de Put, B. Sorée, G. Groeseneken, N. Collaert, and A. V.-Y. Thean

Citation: Applied Physics Letters **105**, 043103 (2014); doi: 10.1063/1.4891348
View online: http://dx.doi.org/10.1063/1.4891348
View Table of Contents: http://scitation.aip.org/content/aip/journal/apl/105/4?ver=pdfcov
Published by the AIP Publishing

Can p-channel tunnel field-effect transistors perform as good as n-channel?

A. S. Verhulst,[1,a)] D. Verreck,[1,2] M. A. Pourghaderi,[1] M. Van de Put,[1,2] B. Sorée,[1,3] G. Groeseneken,[1,2] N. Collaert,[1] and A. V.-Y. Thean[1]
[1]*Imec, Kapeldreef 75, 3001 Leuven, Belgium*
[2]*KU Leuven, 3001 Leuven, Belgium*
[3]*U Antwerpen, 2020 Wilrijk, Belgium*

(Received 16 May 2014; accepted 15 July 2014; published online 29 July 2014)

We show that bulk semiconductor materials do not allow perfectly complementary p- and n-channel tunnel field-effect transistors (TFETs), due to the presence of a heavy-hole band. When tunneling in p-TFETs is oriented towards the gate-dielectric, field-induced quantum confinement results in a highest-energy subband which is heavy-hole like. In direct-bandgap IIIV materials, the most promising TFET materials, phonon-assisted tunneling to this subband degrades the subthreshold swing and leads to at least 10× smaller on-current than the desired ballistic on-current. This is demonstrated with quantum-mechanical predictions for p-TFETs with tunneling orthogonal to the gate, made out of InP, $In_{0.53}Ga_{0.47}As$, InAs, and a modified version of $In_{0.53}Ga_{0.47}As$ with an artificially increased conduction-band density-of-states. We further show that even if the phonon-assisted current would be negligible, the build-up of a heavy-hole-based inversion layer prevents efficient ballistic tunneling, especially at low supply voltages. For p-TFET, a strongly confined n-i-p or n-p-i-p configuration is therefore recommended, as well as a tensily strained line-tunneling configuration.
[http://dx.doi.org/10.1063/1.4891348]

As transistors are further scaled, the optimization of conventional metal-oxide-semiconductor field-effect-transistors (MOSFETs) becomes more and more challenging. Especially the MOSFET's power dissipation problem has resulted in the identification of steep-slope devices of which the tunnel-FET (TFET) is the most promising.[1,2] Carrier injection in TFET is based on band-to-band tunneling (BTBT), and the electrostatic profile at the source (injection) side is such that the injection of part of the hotter carriers is prohibited, resulting in an abrupt on-off switching with sub-60 mV/dec swing.[3] To provide sufficiently high on-current I_{on}, a small effective bandgap in the BTBT injection region is required. This can be realized with either small-bandgap materials or heterojunctions.[4] The I_{on} can also be boosted by optimizing the architecture. A line-TFET architecture has improved performance over a conventional p-i-n architecture, even when pockets are included in the latter.[5]

A key requirement to maintain manageable static leakage, in practical transistor implementations, is the availability of a complementary setup, consisting of a p- and n-TFET. Today, only a limited number of experimental p-TFETs have been realized, such that a thorough evaluation of complementarity is difficult.[1,6–10] However, direct-bandgap IIIV p-TFETs are not expected to reach the same performance (I_{on} for a given supply voltage V_{dd} and off-current I_{off}) as their complementary n-TFETs because of the low density-of-states (DOS) in the conduction band (CB) of these materials, which implies a correspondingly low optimal n-type doping level.[11] This difference can be traced back to the band structure of a direct-bandgap semiconductor which is not fully complementary at zone-center: there is one lowest energy CB, but there are two degenerate highest energy valence bands (VBs), in particular a light-hole (lh) and a heavy-hole (hh) VB. The latter is beneficial for n-TFET by providing a large DOS in the VB,[11] and by analogy, the best material for p-TFET should have a nearby "heavy" indirect bandgap, like GaSb. However, the hh-band also negatively impacts the p-TFET performance as will be outlined in this manuscript.

A crucial distinction between the lh- and hh-VB is that the latter does not couple to the lowest energy CB at zone-center, as can be proven in bulk based on unit cell symmetry properties.[12] Intuitively, the CB s-like wavefunction $|S\rangle$ couples to each VB p-like wavefunction $|X\rangle, |Y\rangle, |Z\rangle$ only in 1 direction ($\langle S|\boldsymbol{p}|X\rangle = \langle S|p_x|X\rangle$), with p the momentum operator. This implies only 1 lh-VB. Ballistic tunneling between the hh-band and the CB is therefore not possible, but phonon-assisted tunneling can exist.[13] So far, no theoretical study has included phonon-assisted tunneling in a TFET configuration where the highest-energy VB is hh-like in the tunneling direction. For configurations like strongly confined nanowires (NWs), the highest-energy VB couples to the lowest-energy CB at zone-center in the direction of the NW axis. In TFETs consisting of these confined NWs or tubes, with tunneling nearly perfectly along the central axis, the phonon-assisted current is predicted to only contribute to increased off-current.[14–16] However, in today's larger-size experimental TFETs, the tunneling direction is not fully parallel to the gate dielectric; and therefore, also tunneling along a direction where the highest-energy VB has hh-like properties is possible. The resulting hh-contribution affects the performance of the p-TFET and the complementarity of TFET in general.

To highlight the impact of the hh-band, a TFET configuration with tunneling orthogonal to the gate is chosen (see line-TFET in Fig. 1).[17] In this direction, the field-induced quantum confinement (FIQC) removes the band degeneracy and brings the hh-band at higher energy than the lh-band

a)Electronic mail: anne.verhulst@imec.be.

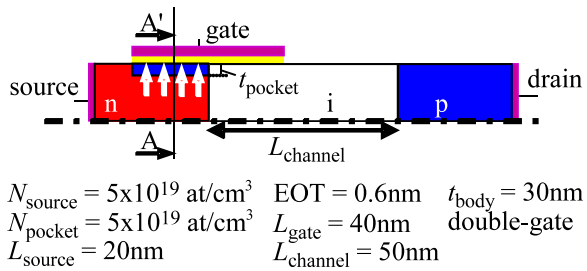

FIG. 1. Schematic of double-gate (DG) pocketed line-TFET. Gate-drain underlap is applied to decrease the ambipolar current.[19] The white arrows indicate the tunneling direction.

(see Fig. 2). The position of the subbands is based on a one-band Schrödinger solver with non-parabolicity correction. The assignment of lh- and hh-band is justified by the modeling work on strongly confined NWs[15,16] as well as quantum wells (QWs)[18] which show pure hh- or lh-like behavior at zone-center. Even though away from zone-center, the top-most band is no longer purely hh-like as it gets admixtures of orbitals coupling to the CB, in this manuscript, the full subband is assumed to be hh-like. This assumption seems justified based on the experimental work on optical transitions in QWs with the electric field in the confinement direction, whereby it is noted that the absorption contribution of the top-most hh-like band is negligible.[18] Transitions between the hh- and conduction band can therefore only be made via phonon-assisted tunneling.[13]

The most promising materials for TFETs are IIIV direct-bandgap materials because of the abundance of lattice-matched heterostructures and the high direct BTBT rates. Even though heterostructures give the best performance,[10] homostructure InP, $In_{0.53}Ga_{0.47}As$, and InAs TFETs are used to illustrate the hh-band impact.[20] To also provide predictions for a p-TFET which does not suffer from the low-eDOS subthreshold swing (SS) degradation, an artificial material with a "heavy-electron" CB is included (Fig. 3; this material is close to GaSb, with its indirect CB edge at 84 meV above its direct one[20]).

Two simulators are combined to assess the impact of the hh-band on the TFET input characteristics (Fig. 4): one simulator for the ballistic BTBT current and another for the phonon-assisted BTBT current calculations, while a one-band 1-dimensional (1D) Schrödinger solver with non-parabolicity correction converts *I-V* curves as needed into quantum-mechanical (QM) solutions including non-

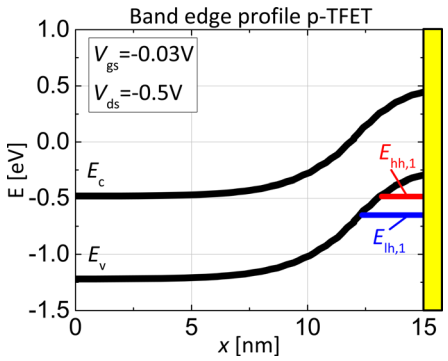

FIG. 2. Electrostatic profile in the source along AA′ of Fig. 1 for a 3 nm pocket $In_{0.53}Ga_{0.47}As$ TFET. The top-most VB subband is hh-like.

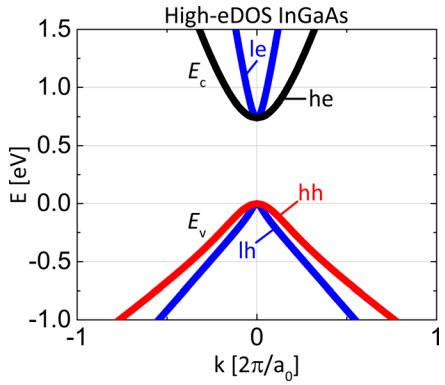

FIG. 3. Bandstructure of artificial high-eDOS $In_{0.53}Ga_{0.47}As$, allowing steeper SS in p-TFET: a "heavy-electron"-band (with hh mass) is added to the $In_{0.53}Ga_{0.47}As$ bandstructure.

parabolicity. The first simulator is semi-classical. It self-consistently solves the Poisson- and drift-diffusion equations with a non-local BTBT model.[21] The latter is a modification of Kane's model implemented with path integrations. Material descriptions include non-parabolicity. Because of the absence of appropriate quantization, the obtained *I–V* curve is voltage-shifted with the FIQC shift[17] calculated based on the one-band solver.

The second simulator is a 2D QM simulator[22] which solves the Poisson-Schrödinger equation self-consistently and calculates the non-local phonon-assisted BTBT current according to the formalism of Ref. 13. The electron-phonon (e-ph) coupling in Ref. 13 is the deformation potential interaction representative for group IV materials. In this article, it is replaced with the in IIIV materials typically stronger polar coupling.[12]

Polar couplings are induced by optical phonons in a lattice of differently charged ions. The corresponding e-ph interaction Hamiltonian $H_{\text{e-ph}}$ is

$$H_{\text{e-ph}} = \sum_{ll'\vec{k}} g_{vlcl'\vec{k}} b_l^\dagger c_{l'} (a_{\vec{k}} + a_{-\vec{k}}^\dagger) + \text{herm. conj.}, \quad (1)$$

with coupling strength $g_{vlcl'\vec{k}}$:

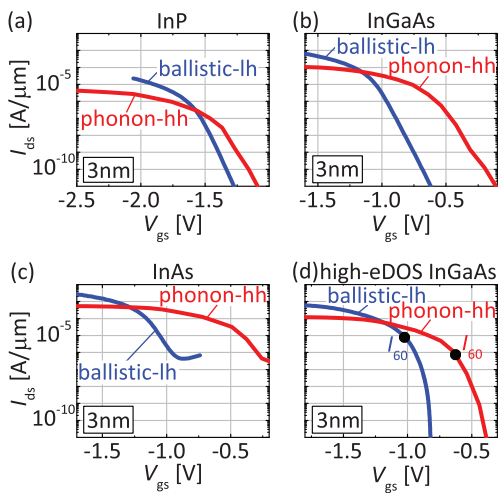

FIG. 4. Simulated input characteristics for (a) InP, (b) InGaAs, (c) InAs, and (d) high-eDOS InGaAs pocketed line-TFETs, $t_{pocket} = 3$ nm, $V_{ds} = -0.5$ V, and WF = 5 eV. Note that a vertically flipped version of the ballistic current curve of (d) is representative for an n-type InGaAs pocketed line-TFET.

$$g_{\mathrm{v}lc l' \vec{k}} = M_k \int_{\nu} \mathrm{d}^3 r \, \phi^*_{\mathrm{v}l}(\vec{r}) \exp(i\vec{k}.\vec{r}) \phi_{\mathrm{c}l'}(\vec{r}), \tag{2}$$

with bulk coupling strength M_k:

$$M_k = \frac{1}{k\nu^{1/2}} \sqrt{2\pi e^2 \hbar \omega_{\mathrm{LO}} \left(\frac{1}{\epsilon_\infty} - \frac{1}{\epsilon_0} \right)}, \tag{3}$$

with v (c) VB (CB), b_l and $c_{l'}$ are the electron annihilation operators in VB and CB states, l and l', respectively, $a_{\vec{k}}$ ($a^\dagger_{\vec{k}}$) the annihilation (creation) operator of a phonon with wavevector $\vec{k}$, $\phi_{\mathrm{v}l}(\vec{r})(\phi_{\mathrm{c}l'}(\vec{r}))$ the electron VB (CB) wavefunctions, ν is the total semiconductor volume, e is the elementary charge, $\hbar$ is the reduced Planck constant, ω_{LO} is the longitudinal optical (LO) phonon frequency, and ϵ_∞ (ϵ_0) is the high-frequency (static) dielectric constant. To obtain a computationally manageable calculation, an average coupling strength $M_{k_{\mathrm{av}}}$ is used. A back-of-the-envelope calculation shows that a good average value is obtained for a wavevector of half the largest relevant k. Very large phonon wavevectors are not relevant, since the effective bandgap for BTBT becomes too large. The value of $k_{\mathrm{av}} = 0.05 \times 2\pi/a_0$, with a_0 the lattice constant, is chosen to determine $M_{k_{\mathrm{av}}}$. Table I lists k_{av} and $M_{k_{\mathrm{av}}} \times \nu^{1/2}$ for the 3 materials used in this article.[20]

The phonon-assisted QM solver of Ref. 13 is further based on the effective mass approximation. Since the non-parabolicity of the CB is typically significant in IIIV materials,[23] the gate-source voltage V_{gs} required for alignment of the hh-subband level to the electron Fermi level will be overestimated and the correspondingly larger electric field will result in current-overestimation too. The following linear interpolation and current rescaling is performed to extract the "non-parabolic" input characteristics. Based on a one-band Schrödinger solver, the electrostatic potential profile orthogonal to the gate is determined for 6 predefined energetic distances between the hh-subband level and the electron Fermi level or CB edge in the source. The 6 conditions range from onset of BTBT at overlap of the hh-subband to the CB (condition of Fig. 2) to alignment of the hh-subband to the electron Fermi level in the source. Two parameters are extracted for the 6 conditions and for both the parabolic and non-parabolic CB assumption: the maximum electric field E_{max} in the source and V_{gs}. A linear interpolation of the V_{gs} values is performed, combined with a rescaling of the current values proportional to the tunneling rate at uniform E_{max}

$$I \sim E_{\mathrm{max}}^{2.5} \exp(-B_{\mathrm{BTBT}}/E_{\mathrm{max}}), \tag{4}$$

with B_{BTBT} a material-dependent tunneling parameter.[24] This E_{max}-based simplified rescaling results in an overestimation of the phonon-assisted hh-based current.

TABLE I. Reduced average bulk polar coupling strength $M_{k_{\mathrm{av}}} \times \nu^{1/2}$.

	InP	InGaAs	InAs
k_{av} (m^{-1})	5.4×10^8	5.4×10^8	5.2×10^8
$M_{k_{\mathrm{av}}} \times \nu^{1/2}$ ($\mathrm{Jm}^{3/2}$)	3.2×10^{-33}	2.2×10^{-33}	2.2×10^{-33}

The line-TFET predictions are shown in Fig. 4 for a configuration with a 3 nm pocket. An observable current to the hh-subband adds to the desired ballistic tunneling current for all materials. The total current achieved in a given voltage window V_{dd} starting at V_{onset} ($@I_{\mathrm{off}} = 50\,\mathrm{pA}/\mu\mathrm{m}$) is smaller than if only lh-based current were present. For example, in Fig. 4(d), taking $V_{\mathrm{dd}} = 0.5$ V, the current-prediction based on the ballistic component only is about 200 μA/μm ($V_{\mathrm{onset}} \approx -0.8$ V), while the prediction when both phonon-based and ballistic currents are taken into account is about 20 μA/μm ($V_{\mathrm{onset}} \approx -0.4$ V), with a corresponding I_{60} degradation from 5 μA/μm to 1 μA/μm.[3] The hh-based current therefore degrades the TFET's input characteristics. The shift of the hh-current with respect to the lh-current is larger for materials with smaller masses, despite the smaller bandgaps and hence smaller required band bendings. The shift is also larger for thinner pockets, due to the increased FIQC, but the impact is limited ($\leq$100 mV shift decrease for 5 nm pocket TFETs). The shift for high-eDOS $In_{0.53}Ga_{0.47}As$ is smaller than for $In_{0.53}Ga_{0.47}As$ due to the smaller electric fields at turn-on and hence the smaller FIQC.

If the assumption that the hh-band is not coupled to the CB beyond zone-center is removed, then it is to be expected that the ballistic current can start closely beyond the onset of phonon-assisted tunneling. For transitions to the hh-like band, the hh-based (phonon-assisted) component is expected to remain dominant, but an lh-based (ballistic as well as phonon-assisted) component will also appear. Overall, the impact of orbital mixing is therefore expected to be a smoothening of the I-V characteristics compared to the in Fig. 4 presented sum of the purely lh-based ballistic current and the purely hh-based phonon-assisted current.

The presence of a hh-like subband as top-most VB is also problematic for direct-bandgap materials with negligible phonon-assisted tunneling, e.g., tensile strained (non-polar) Ge. This is illustrated with a full QM solver, such that energetic positions of hh- and lh-subbands are properly incorporated. Because of solver restrictions, the illustration can not be done for phonon-assisted hh-based current versus ballistic lh-current, but is done versus phonon-assisted lh-based current (Fig. 5), which is representative as well for illustrating

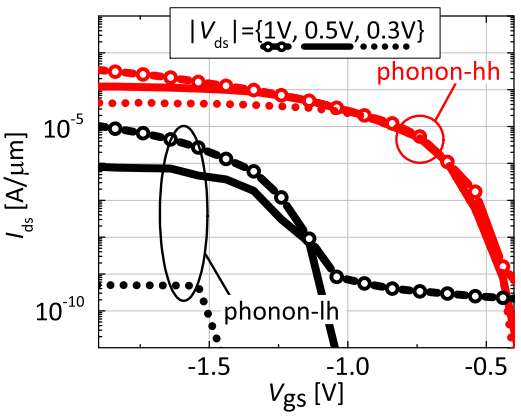

FIG. 5. Simulated *I-V* curves for a high-eDOS InGaAs line-TFET with 3 nm pocket. A parabolic band assumption is used for the lh band. The decrease of current with decreasing $|V_{\mathrm{ds}}|$ is larger for lh-based than for hh-based current.

the hh-based level pinning. To have observable lh-based currents and since the pinning impact is independent of the magnitude of the phonon-assisted current, polar high-eDOS InGaAs is used in Fig. 5. Note that the phonon-assisted lh-based current is not added to Fig. 4 as it is always smaller than the ballistic lh-based current. As shown in Fig. 5, when $|V_{ds}|$ decreases, the lh-based current decreases more strongly than the hh-based current. This is because an inversion layer builds up in the hh-subband, limiting band bending in the semiconductor, once the hh-subband edge is energetically close to the hole Fermi level, with the latter set by the p-type drain voltage. The energetic distance from the lh-subband level to the source electron Fermi level is therefore pinned by the hole Fermi level in the hh-subband, such that lh-BTBT is suppressed. From $|V_{ds}| = 1$V to $|V_{ds}| = 0.5$V, part of the lh-based current decrease is due to inefficient tunneling into partially filled CB states. At $|V_{ds}| = 0.3$V, overlap between the lh-subband and the CB is marginal, which is reflected in the strong deterioration of the lh-based current. This pinning of the band bending and the resulting decrease of the lh-based current is not included in Fig. 4. The overall impact of the hh-band is therefore even worse than anticipated by Fig. 4.

Heterostructure stacks of large-bandgap materials can help to increase the CB DOS while maintaining favorable tunneling rates. However, heterostructure line-TFETs[25] suffer from the same parasitics as the presented homostructure line-TFETs. In the tunneling direction, which is the confinement direction of the thin hetero-material, the top-most VB has hh-properties and no ballistic CB coupling.

In confined NWs, however, tunneling happens parallel to the gate. In this direction, the top-most VB couples ballistically to the CB.[15] Tensile strain along the NW axis enhances this favorable band alignment.[16] Biaxial tensile strain can also be applied to line-TFET configurations to create a top-most VB in the direction of tunneling which couples ballistically to the CB.

In conclusion, in TFET architectures in which BTBT is oriented towards the gate dielectric, direct-bandgap p-TFETs perform worse than n-TFETs. We have shown that a parasitic phonon-assisted tunneling component appears a few 100 mV before the desired ballistic tunneling component onset in such IIIV p-TFETs, with no equivalent of this phenomenon in n-TFETs. The onset of this parasitic current with respect to the onset of the desired current is larger with decreasing bandgap and effective masses and with increasing FIQC. Even if non-polar (non-IIIV) materials are used, such that the phonon-assisted current becomes negligible, the desired ballistic lh-based current degrades and for supply voltages below 0.3 V may become negligible, due to the hh-band presence. The ideal material in the BTBT injection region of a p-TFET has a large DOS in the CB and its top-most VB at onset of tunneling couples ballistically to the CB. Future p-TFET designs should therefore be limited to strongly confined n-i-p or n-p-i-p TFETs or biaxially tensily strained line-TFETs, by preference with heterostructures in the BTBT region.

This work was supported by imec's industrial application program. D. Verreck acknowledges the support of a Ph.D. stipend from the Institute for Promotion of Innovation through Science and Technology in Flanders (IWT).

[1]A. Seabaugh and Q. Zhang, Proc. IEEE **98**, 2095 (2010).
[2]A. Ionescu and H. Riel, Nature **479**, 329 (2011).
[3]W. Vandenberghe, A. Verhulst, B. Sorée, W. Magnus, G. Groeseneken, Q. Smets, M. Heyns, and M. Fischetti, Appl. Phys. Lett. **102**, 013510 (2013).
[4]A. Verhulst, W. Vandenberghe, K. Maex, S. D. Gendt, M. Heyns, and G. Groeseneken, IEEE Electron Device Lett. **29**, 1398 (2008).
[5]D. Verreck, A. Verhulst, K.-H. Kao, W. Vandenberghe, K. D. Meyer, and G. Groeseneken, IEEE Trans. Electron Devices **60**, 2128 (2013).
[6]F. Mayer, C. L. Royer, J.-F. Damlencourt, K. Romanjek, F. Andrieu, C. Tabone, B. Previtali, and S. Deleonibus, Int. Electron Devices Meet. **2008**, 1.
[7]D. Leonelli, A. Vandooren, R. Rooyackers, A. Verhulst, S. D. Gendt, M. Heyns, and G. Groeseneken, Jpn. J. Appl. Phys. **49**, 04DC10 (2010).
[8]R. Gandhi, Z. Chen, N. Singh, K. Banerjee, and S. Lee, IEEE Electron Devices Lett. **32**, 1504 (2011).
[9]K. Moselund, H. Schmid, C. Bessire, M. Bjork, H. Ghoneim, and H. Riel, IEEE Electron Device Lett. **33**, 1453 (2012).
[10]B. Rajamohanan, D. Mohata, Y. Zhu, M. Hudait, Z. Jiang, M. Hollander, G. Klimeck, and S. Datta, J. Appl. Phys. **115**, 044502 (2014).
[11]W. Vandenberghe, A. Verhulst, K.-H. Kao, K. D. Meyer, B. Sorée, W. Magnus, and G. Groeseneken, Appl. Phys. Lett. **100**, 193509 (2012).
[12]P. Yu and M. Cardona, *Fundamentals of Semiconductors*, 3rd ed. (Springer, 2001), p. 69(2.6.1), 121(3.3).
[13]W. Vandenberghe, B. Sorée, W. Magnus, and M. Fischetti, J. Appl. Phys. **109**, 124503 (2011).
[14]S. Koswatta, M. Lundstrom, and D. Nikonov, Appl. Phys. Lett. **92**, 043125 (2008).
[15]M. Luisier and G. Klimeck, J. Appl. Phys. **107**, 084507 (2010).
[16]F. Conzatti, M. Pala, D. Esseni, E. Bano, and L. Selmi, IEEE Trans. Electron Devices **59**, 2085 (2012).
[17]W. Vandenberghe, B. Sorée, W. Magnus, G. Groeseneken, and M. Fischetti, Appl. Phys. Lett. **98**, 143503 (2011).
[18]D. A. B. Miller, J. S. Weiner, and D. S. Chemla, IEEE J. Quantum Electron. **22**, 1816 (1986).
[19]A. Verhulst, W. Vandenberghe, K. Maex, and G. Groeseneken, Appl. Phys. Lett. **91**, 053102 (2007).
[20]See http://www.ioffe.ru/SVA/NSM/Semicond/ for semiconductor material parameters.
[21]Synopsys, SentaurusDevice, v. 2012.06.
[22]W. Vandenberghe, B. Sorée, W. Magnus, M. Fischetti, A. Verhulst, and G. Groeseneken, Int. Electron Devices Meet. **2011**, 5.3.1.
[23]V. Altschul, A. Fraenkel, and E. Finkman, J. Appl. Phys. **71**, 4382 (1992).
[24]E. Kane, J. Appl. Phys. **32**, 83 (1961).
[25]G. Zhou, R. Li, T. Vasen, M. Qi, S. Chae, Y. Lu, Q. Zhang, H. Zhu, J.-M. Kuo, T. Kosel, M. Wistey, P. Fay, A. Seabaugh, and H. Xing, Int. Electron Devices Meet. **2012**, 32.6.1.